1-1-2019

Electrical properties of yttrium calcium oxyborate crystal annealed at high temperature and low oxygen partial pressure

Shiwei Tian
Shandong University

Lili Li
Shandong University

Feifei Chen
Shandong University

Chao Jiang
Shandong University

Fapeng Yu
Shandong University

See next page for additional authors

Electrical properties of yttrium calcium oxyborate crystal annealed at high temperature and low oxygen partial pressure

Abstract

The yttrium calcium oxyborate crystal (YCa 4 O(BO 3) 3 , YCOB) has been actively studied for high-temperature piezoelectric sensing applications. In this work, the stability of electric properties of YCOB crystal annealed in critical conditions (high-temperatures of 900-1100 °C with a low oxygen partial pressure of 4 x 10 −6 atm for 24 h) was investigated and the recovery mechanism for the electrical resisitivity, dielectric permittivity and dielectric loss were studied, taking advantage of the X-ray photoelectron spectra and the first principle calculations. The electrical resistivity of the annealed YCOB crystal was slightly decreased when compared to the pristine counterpart, being (2-5) x 10 7 Ω cm at 850 °C. The dielectric permittivity and dielectric loss were found to increase after annealing, showing recoverable behaviours after thermal treatment above 650 °C in air. The calculated vacancy formation energy indicate that the oxygen vacancy is the dominant defects in YCOB. The formation of oxygen vacancy weakens the chemical bonding strength between B (Ca or Y) and O atoms, introduces extra donor levels in the band gap, which excites the electrons to conduction band more easily thus enhances the electrical conductivity and dielectric loss. The recovered electrical properties are believed to be associated with the reduced vacancy defects at elevated temperatures in air.

Disciplines

Engineering | Physical Sciences and Mathematics

Publication Details

Tian, S., Li, L., Chen, F., Jiang, C., Yu, F., Li, Y., Duan, X., Wang, Z., Zhang, S. & Zhao, X. (2019). Electrical properties of yttrium calcium oxyborate crystal annealed at high temperature and low oxygen partial pressure. Journal of Materiomics, 5 363-371.

Authors

Shiwei Tian, Lili Li, Feifei Chen, Chao Jiang, Fapeng Yu, Yanlu Li, Xiulan Duan, Zhengping Wang, Shujun Zhang, and Xian Zhao

Journal of Materiomics 5 (2019) 363–371

Contents lists available at ScienceDirect

Journal of Materiomics

journal homepage: www.journals.elsevier.com/journal-of-materiomics/

Electrical properties of yttrium calcium oxyborate crystal annealed at high temperature and low oxygen partial pressure

Shiwei Tian [a], Lili Li [a], Feifei Chen [a], Chao Jiang [a], Fapeng Yu [a, *], Yanlu Li [a, **], Xiulan Duan [a], Zhengping Wang [a], Shujun Zhang [b], Xian Zhao [a]

[a] State Key Laboratory of Crystal Materials, Advanced Research Center for Optics of Shandong University, Jinan, 250100, China
[b] ISEM, Australia Institute of Innovative Materials, University of Wollongong, Wollongong, NSW, 2500, Australia

ARTICLE INFO

Article history:
Received 11 December 2018
Received in revised form
26 January 2019
Accepted 12 February 2019
Available online 13 February 2019

Keywords:
YCOB crystal
Recoverable dielectric properties
First principle calculations

ABSTRACT

The yttrium calcium oxyborate crystal ($YCa_4O(BO_3)_3$, YCOB) has been actively studied for high-temperature piezoelectric sensing applications. In this work, the stability of electric properties of YCOB crystal annealed in critical conditions (high-temperatures of 900–1100 °C with a low oxygen partial pressure of 4×10^{-6} atm for 24 h) was investigated and the recovery mechanism for the electrical resisitivity, dielectric permittivity and dielectric loss were studied, taking advantage of the X-ray photoelectron spectra and the first principle calculations. The electrical resistivity of the annealed YCOB crystal was slightly decreased when compared to the pristine counterpart, being $(2–5) \times 10^7\ \Omega \cdot$cm at 850 °C. The dielectric permittivity and dielectric loss were found to increase after annealing, showing recoverable behaviours after thermal treatment above 650 °C in air. The calculated vacancy formation energy indicates that the oxygen vacancy is the dominant defects in YCOB. The formation of oxygen vacancy weakens the chemical bonding strength between B (Ca or Y) and O atoms, introduces extra donor levels in the band gap, which excites the electrons to conduction band more easily thus enhances the electrical conductivity and dielectric loss. The recovered electrical properties are believed to be associated with the reduced vacancy defects at elevated temperatures in air.

1. Introduction

The aerospace, automotive and power plants industries have expressed particular interests in high-temperature piezoelectric sensors for structure health monitoring (SHM) over a broad temperature range. Such kind of sensors are usually required to possess the merits of high durability and stability in critical environment, such as high temperatures, low pO_2, vacuum, in addition to high sensitivity [1].

For practical piezoelectric sensing at high temperatures (>800°C), the durability and stability of the piezoelectric devices are impacted by the intrinsic electrical properties of piezoelectric materials, which can affect the stability of their electro-elastic properties, thus determines the usages temperature range of piezoelectric sensors. Particularly for sensors based on direct piezoelectric effect, such as piezoelectric vibration sensor and accelerometer etc., one of the basic requirements is the *RC* time constant (Equation (1), where *R* is electrical resistance and *C* is capacitance of the device). It is known that the time of the piezoelectric charge maintained in a sensor is proportional to the *RC* time constant [2,3]. The minimum useful frequency of a piezoelectric sensor, which is known as the lower limiting frequency (f_{LL}), is inversely proportional to the *RC* time constant [1]. If the operational frequency is lower than the f_{LL} value of the sensor, the produced piezoelectric charge will drain off as leakage current before it can be detected. In addition, the high temperature environment is generally accompanied by other challenges, such as vacuum, low pO_2, radiation hard, and corrosion etc. [4]. These harsh environments could affect the durability of electro-elastic properties of high temperature piezoelectric crystals [5,6]. Especially the combination of high temperature and low pressure/low pO_2 will induce oxygen vacancies in the oxide crystal, which will contribute to the conductivity and reduce the electrical resistivity.

$$f_{LL} = \frac{1}{2\pi RC} \tag{1}$$

* Corresponding author.
** Corresponding author.
E-mail addresses: fapengyu@sdu.edu.cn (F. Yu), liyanlu@sdu.edu.cn (Y. Li).
Peer review under responsibility of The Chinese Ceramic Society.

https://doi.org/10.1016/j.jmat.2019.02.007

Of all the high-temperature piezoelectric materials, the $GaPO_4$, langasite (LGS), AlN and YCOB single crystals have been extensively studied [7–26] The trigonal $GaPO_4$ crystal was found to exhibit high electrical resistivity ($10^7\,\Omega\cdot$cm @ 800 °C) and high stability of mechanical and piezoelectric properties up to the α-β phase transition near 970 °C. However, the performance would be decreased due to the increase of structural disorder at temperatures above 700 °C [1,10,11]. The LGS crystal was reported to possess the same crystal symmetry as $GaPO_4$ and showed no phase transition prior to its melting point (~1470 °C), however, the sensing performance would be restricted by its low electrical resistivity at high-temperatures ($<10^5\,\Omega\cdot$cm @ 800 °C), resulted from the ionic conductivity [15–18]. The hexagonal AlN crystal grown by physical vapor transport method was reported to show high electrical resistivity ($10^{11}\,\Omega\cdot$cm @ 800 °C) and good temperature stability of piezoelectric activity up to 1000 °C. Similar to AlN crystal, the monoclinic YCOB crystal shows outstanding electro-elastic properties and electrical resistivity [19–21]. The effective piezoelectric coefficient d_{33} was found to be 6–7 pCN^{-1} at room temperature, slightly higher than the LGS, $GaPO_4$ and AlN crystals. Besides, the resistivity along the physical Y axis was reported to be $10^8\,\Omega\cdot$cm at 800 °C, one order higher than the $GaPO_4$ crystal and more than two orders higher than LGS crystal [1]. The *RC* time constant for YCOB crystal was obtained to be on the order of 0.2 ms, one to two orders of magnitude higher than LGS and $GaPO_4$ crystals [22]. Based on the YCOB crystal, different prototypes of piezoelectric sensors were fabricated with reliable sensing signal around 1100 °C [19, 23–26].

Nevertheless, the successful fabrication of YCOB based piezoelectric sensors at high temperature, the stability and reliability of the electrical properties under combined critical environments (high-temperature and low pO_2, or vacuum), however, are very limited [5]. In this report, the temperature stabilities of the electric resistivity and dielectric properties of YCOB crystals annealed at temperatures of 900–1100 °C combined with a low oxygen partial pressure of 4×10^{-6} atm were studied, moreover, the influence mechanism was discussed.

2. Structure of YCOB crystal

The YCOB crystal and its isomorphs belong to monoclinic crystal symmetry with C_m space group. The structure of ReCOB crystal has been descripted in details [27,28]. In YCOB crystal, there are two types of Ca-O polyhedra, one type Y-O polyhedron and two types B-O triangle planes with six kinds of oxygen sites (O_1, O_2, O_3, O_4, O_5, and O_6), as shown in Fig. 1. The average bond length for Ca_1-O was calculated to be 2.34369 Å, higher than that in Ca_2-O polyhedron (2.33792 Å) [29].

3. Experimental and calculation sections

3.1. Evaluation of electrical resistivity and dielectric properties

High quality YCOB crystals were grown by using the Czochralski pulling method [10–12] along the <010> direction, which was parallel to the crystallographic b-axis. The starting materials were high purity (99.99%) Y_2O_3, $CaCO_3$ and H_3BO_3 powders. The powders were weighted in stoichiometric ratio with an excess of 1~2wt% H_3BO_3. Polycrystalline YCOB compounds synthesized by solid state reaction method were used for single crystal growth. The pulling and rotation speeds were controlled to be 0.45 mm/h and 16~20 rpm, respectively during the single crystal growth process. The grown YCOB crystal was oriented and sliced into Y-cut samples with dimension of 10(X) ×10(Z)×1.2(Y) mm^3. These crystal samples were annealed at critical conditions (900–1100 °C and a low oxygen partial pressure of 4×10^{-6} atm for 24 h) to study the stability of electrical resistivity and relative dielectric permittivity. The main facets perpendicular to the physical Y axis were sputtered with 200 nm platinum films using a sputter coater (BAL-TEC, SCD 050). The electrical resistance of the surface electrodes was measured to be <5Ω. For comparison, the annealed samples were further thermal treated in air for 0–180 min at 650 °C. The electrical resistance R (R = U/I) was obtained by measuring the current of the Y-cut

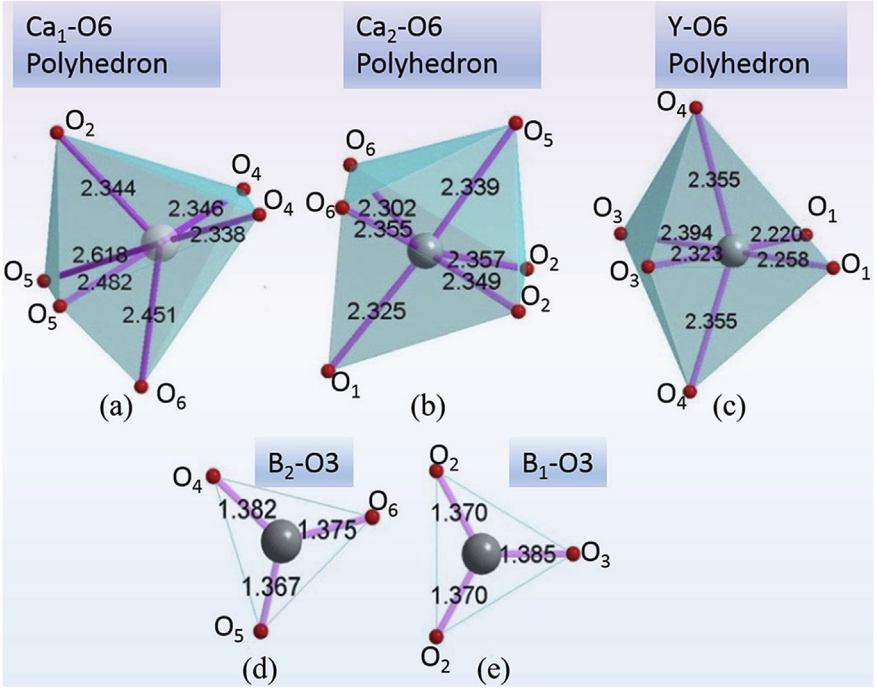

Fig. 1. Bond lengths and the polyhedron models of YCOB crystal. (a) Ca_1-O polyhedron; (b) Ca_2-O polyhedron; (c) Y-O polyhedron; (d) B_2-O triangle and (e) B_1-O triangle.

sample under 100 V using a source meter (Keithley 2410C) in the temperature range of 650–850 °C. The electrical resistivity was evaluated using Equation (2), where ρ, U, I, A, and t are the electrical resistivity, applied voltage, measured current, area and thickness of the YCOB sample, respectively. The capacitance and dielectric loss at different frequencies were recorded by using a multi-frequency LCR meter (Agilent 4263B). The relative dielectric permittivity was evaluated by Equation (3), where C and ε_0 represent the capacitance of the crystal sample and dielectric permittivity in vacuum, respectively.

$$\rho = \frac{UA}{It} \tag{2}$$

$$\varepsilon_{22}/\varepsilon_0 = \frac{Ct}{A\varepsilon_0} \tag{3}$$

3.2. Raman study

YCOB crystal samples with dimension of $5 \times 5 \times 1\ mm^3$ (Y-cut) were prepared and polished for Raman spectra characterization at room temperature. Raman tests for the pristine and annealed YCOB crystal samples were conducted on a confocal Raman spectroscopy (LabRAM HR800) in a back scattering configuration using a 532 nm excitation laser. The Raman spectra with precision of ~1 cm^{-1} was collected from 100 cm^{-1} to 700 cm^{-1}.

3.3. XPS analysis

The X-ray photoelectron spectra (XPS) were performed on an X-ray photoelectron spectrometer (Thermo-Fisher ESCALAB 250) by mono-chromatized Al K X-ray radiation in ultrahigh vacuum of $<10^{-7}$ Pa. The binding energies were calibrated via the C 1s peak (284.6 eV) of carbon impurities as a reference and the peaks were de-convoluted after subtracting the background with a mixed Gaussian-Lorentzian function. The results were analyzed by using the Advantage software.

3.4. First-principle calculations

The theoretical calculations were performed by employing Vienna *ab* initio Simulation Package [30,31] implementation of density functional theory (DFT) combining with the projector-augmented-wave (PAW) formalism [32]. The O $2s^2 2p^4$, B $2s^2 2p^1$, Y $4d^1 5s^2$, and Ca $4s^2$ states were treated as the valence electrons. In the calculations, the electronic wave functions were expanded in plane waves up to a cutoff energy of 300 eV. Particularly, the local-density approximation (LDA) with the Ceperley-Alder and Perdew and Zunger forms were used to describe the exchange and correlation potential [33,34]. All the atomic positions, lattice parameters and properties were calculated by LDA. The force convergence criterion was 0.01 eV/Å. The Monkhorst-Pack [35] k-point meshes were employed to sample the Brillouin zones for all the calculations, where $3 \times 2 \times 6$ Monkhorst-Pack k-point was used in this work based on the convergence meshes. The optimized lattice parameters for YCOB in this study are a = 7.99 Å, b = 15.90 Å and c = 3.47 Å with the variation of 1.00%, 0.69% and 1.70% respectively as compared to the experimental measured values (a=8.07, b=16.01, and c=3.53 Å, referred from PDF#50-0403), indicating that the calculation parameters used here are reasonable.

The oxygen vacancy (V_O) model was constructed by removing one O atom from a monoclinic YCOB unit cell that contains 36 atoms. We could get the yttrium vacancy (V_Y), calcium vacancy (V_{Ca}), and boron vacancy (V_B) models following the same way. The vacancy formation energy could be evaluated using the following Equation [36],

$$E_V = E_D + \mu_i - E_p \tag{4}$$

where E_D and E_p are the total energies of the supercells with and free of a vacancy defect, u_i corresponds to the chemical potential of the corresponding atoms. The chemical potentials of B, Ca, and Y atoms were calculated by using their corresponding elemental phases, i.e., B (Rhombohedral: $\bar{3}m$), Ca (Cubic: $m\bar{3}m$), Y (Hexagonal: $6/mmm$). Furthermore, we utilized an O_2 molecular as our model structure with a dimension of $10 \times 10 \times 10\ Å^3$, in which the chemical potential of oxygen atom was set to be half total energy of the O_2.

4. Experimental results and discussion

4.1. Variations of electrical resistivity and dielectric properties

The temperature dependent behaviors of the electrical resistivity for the pristine and annealed YCOB samples were investigated. Results are given in Fig. 2. It was found that the electrical resistivity ρ_{22} of all the YCOB samples decreased with increasing annealing temperatures. The electrical resistivity of the pristine YCOB crystal at 850 °C is $5.0 \times 10^7\ \Omega \cdot cm$, slightly decreased to $2.0 \times 10^7\ \Omega \cdot cm$ after annealing at 1100 °C (under a low oxygen partial pressure of 4×10^{-6} atm for 24 h). Interestingly, the resistivity of the annealed crystal was found to show an increase after thermal treatment at 800°C in air (marked as 800°C* in Fig. 2), being on the order of $3 \times 10^7\ \Omega \cdot cm$ at 850°C). The activation energy was calculated via the Arrhenius law (Equation (5)), where ρ, A, Ea, K, and T represent the electrical resistivity, pre-exponential factor, activation energy, the molar gas constant and absolute temperature, respectively.

$$\rho = Ae^{-E_a/KT} \tag{5}$$

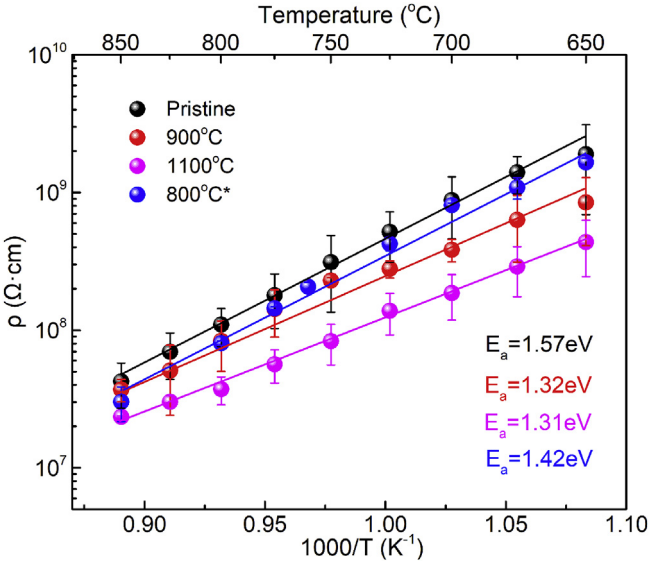

Fig. 2. The temperature dependence of electrical resistivity for the pristine, annealed (900 °C and 1100 °C under a low oxygen partial pressure of 4×10^{-6} atm for 24 h) and thermal treated (800 °C in air, marked as 800 °C*) YCOB crystals.

It was obtained that the activation energy decreased with increasing annealing temperature. The activation energy for YCOB crystal annealed at 1100 °C was calculated to be 1.31 eV, slightly lower than that of the pristine YCOB sample (1.57 eV). Notably, the activation energy of the thermal treated crystal is 1.42eV, higher than the annealed samples but lower than that of pristine crystal. The activation energy of the YCOB crystal was assumed to be associated with the oxygen vacancy (one type of long-range defect) [37] and the decreased chemical bonding strength in YCOB crystal (M-O bond, M represents the atoms Y, Ca and B), induced by annealing under critical conditions.

The frequency dependent behaviors of the relative dielectric permittivity and dielectric loss $\tan\delta_{22}$ for the pristine and annealed Y-cut YCOB crystal samples (at 1100 °C and a low oxygen partial pressure of 4×10^{-6} atm for 24 h) with different thermal treatment times (650 °C in air for 0-180min) were studied. Results are presented in Figs. 3 and 4. It was found that the relative dielectric permittivity of the annealed YCOB crystal was 15.3, higher than that of the pristine samples, being 14.0 at 1 kHz. The dielectric permittivities decrease with extending of the thermal treatment time in air (0–180 min), as shown in Fig. 3. It is interesting to note that the dielectric permittivity of the annealed sample after thermal treatment at 650 °C for 180 min approaches to that of the pristine sample at the same temperature. The dielectric permittivity of the pristine YCOB crystal suffering from annealing under combined challenge conditions can be recovered after thermal treatment in air. Similar trend was also obtained for the dielectric loss $\tan\delta_{22}$, as shown in Fig. 4. Experimental results further reveal that the recovery time of the annealed YCOB crystal at temperatures over 650°C could be shortened, being less than 180 min.

4.2. Raman analysis

From the crystallography point of view, the compound and its isomorphs have comparable lattice parameters and vibration spectra, where the lattice dynamics possess many common characteristics [38,39]. In this work, the Raman spectra were used to study the microstructure variation of YCOB crystals annealed under critical conditions. Fig. 5 presents the un-polarised Raman spectra of the Y-cut YCOB crystal annealed at 1100 °C and low oxygen partial pressure of 4×10^{-6} atm for 24 h, together with the pristine sample for comparison. The Raman peaks of the annealed sample (1100 °C) shift slightly toward the red region by ~2 cm^{-1} (red line in Fig. 5) and the intensities of Raman peaks decrease over the tested wave-number range of 150–700 cm^{-1}, especially at 180 cm^{-1}, 247 cm^{-1} and 338 cm^{-1} (marked by blue ellipses). The red shift in Raman spectra usually corresponds to the decrease of chemical bonding strength [27,40,41]. According to the structure of YCOB crystal, the average bond length in Ca_1-O polyhedron is longer than that in Ca_2-O polyhedron, indicating the average chemical bonding strength of Ca_1-O polyhedron is weaker than that in the Ca_2-O polyhedron. From this point of view, the Raman peaks at 130 cm^{-1} and 180 cm^{-1} should be assigned to the Ca_1-O and Ca_2-O polyhedron, respectively. Therefore, it is reasonable to conclude that the decreased intensities in Raman peaks around 180 cm^{-1}, 247 cm^{-1} and 338 cm^{-1} for the annealed sample are associated with the weakened chemical bonding strength of Ca-O in Ca_2-O polyhedron, B-O in B-O triangle and the Y-O in Y-O polyhedron during the annealing process, respectively.

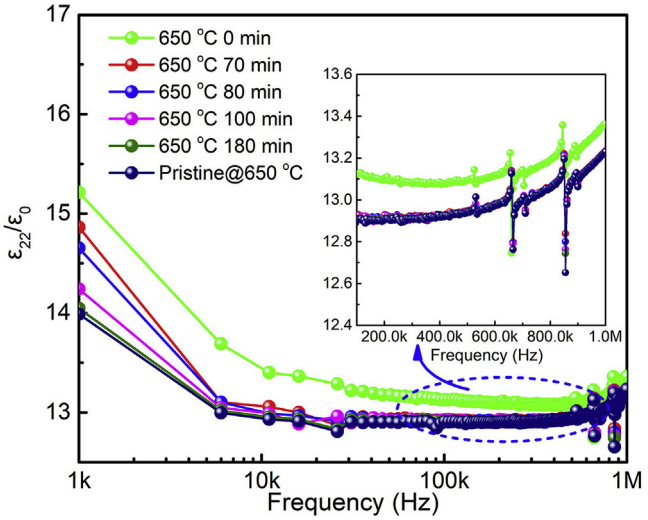

Fig. 3. The frequency dependent behaviour of relative dielectric permittivity for the annealed YCOB crystal with different thermal treatment times in air (the abnormal peaks over the range of 400 kHz–1 MHz in small insert are associated with the resonant and anti-resonant frequencies).

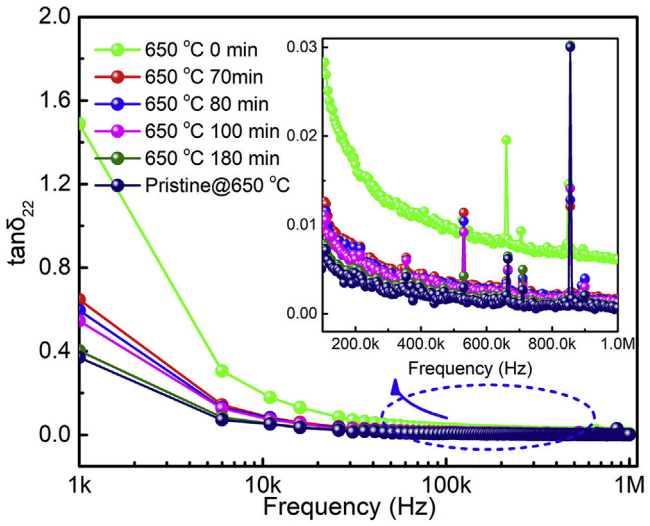

Fig. 4. The frequency dependent behaviour of dielectric loss for the annealed YCOB crystal sample with different thermal treatment times in air (the abnormal peaks over the range of 400 kHz–1 MHz in small insert are associated with the resonant and anti-resonant frequencies).

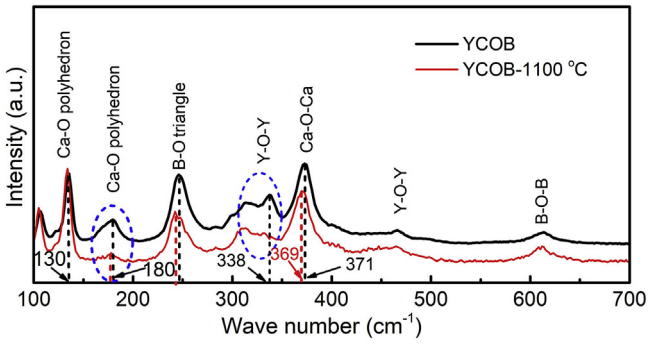

Fig. 5. Raman spectra of YCOB samples measured at room temperature. The black line in black is the Ra-man spectrum of pristine YCOB sample and red line in red is the spectrum of the YCOB sample suffered from after annealing at 1100 °C (1100 °C and 2×10^{-5} atm for 24 h).

4.3. XPS analysis

The binding energy (BE) difference ΔBE(O-M)=BE(O1s)-BE(M), where M is a representative metal core level) is an important parameter to evaluate the chemical bonding characterization. It has successful applications on many cations in oxide crystals [42–44]. It is known that when a M-O bond formed, it is difficult to loss an electron from the metal atom since the valance electron density of the metal atom would shift toward oxygen atom. In addition, the binding energy of the metal atom would increase [45,46]. Consequently, when the chemical bond (M-O) gets stronger, the binding energy of metal would increase, while the binding energy of O 1s would decrease. As a result, the value of ΔBE(O-M) would decrease. In contrast, lower binding energy of M and higher binding energy of O 1s contribute to a higher ΔBE(O-M) value, with the M-O chemical bonding strength decreasing. Though the X-ray photoelectron spectra (XPS) tests give the information of crystal surface with depth below 10nm, it directly reflects the variations of electric structure of the YCOB crystals before and after annealing. Figs. 6 and 7 present the X-ray photoelectron spectra (XPS) results of B 1s, O 1s, Ca 2p, and Y 3d for the annealed YCOB crystals (1100 °C and low oxygen partial pressure of 4×10^{-6} atm for 24 h), together with the pristine and thermal treated (800 °C in air for 0.5 h) samples for comparison. It was observed that the binding energies of B 1s, Ca 2p, and Y 3d show a decrease trend (0.07 eV–0.56 eV) when compared to pristine sample (Fig. 6(a), (c) and (d)), while the binding energy for the O 1s shown contrary trend (Fig. 6(b)), leading to an increased ΔBE(O-M) value. According to chemical bonding analysis above, we can conclude that the chemical bonding strength of M-O was weakened in YCOB crystal after annealing.

It is noticed that the intensities of the XPS peaks for all the elements are decreased after annealing, indicating that all the atoms could escape from the YCOB crystal under critical conditions. Meanwhile, the binding energies of the B 1s, Ca 2p, and Y 3d for the annealed YCOB crystal were also found to exhibit a decreasing trend. However, these values were increased after further thermal treatment in air (800 °C for 0.5 h), showing a recovered behavior. Similar tendency was also observed in the variations of area percentages of the XPS peaks. The area percentages of the O, B, Y and Ca atoms for the pristine YCOB crystal were 54.76%, 16.11%, 6.74% and 22.39%, respectively, shifted to 49.33%, 17.55%, 7.06% and 26.06% after annealing (1100 °C and a low oxygen partial pressure of 4×10^{-6} atm for 24 h). The variations were on the order of −7.93%, 5.85%, 5.22% and 12.67%, respectively. Interestingly, the area percentages of XPS peaks for

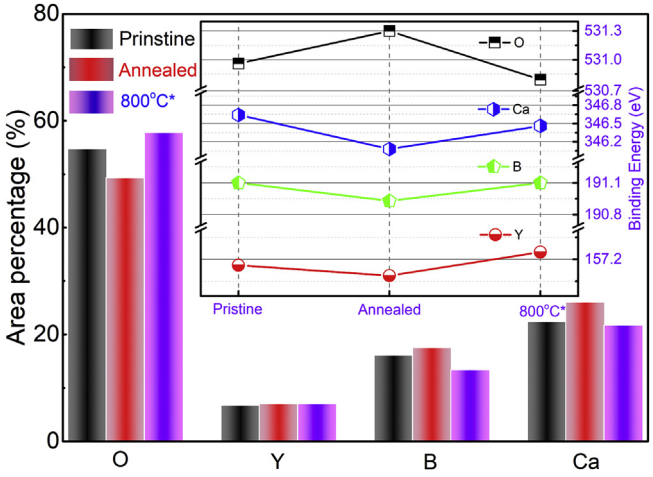

Fig. 7. The variations of area percentages of the atoms (O, Y, B, and Ca atoms) upon pristine, annealed and thermal treated (thermal treated at 800 °C in air for 0.5 h) measured by XPS. The small inset gives the variation of binding energies for different atoms.

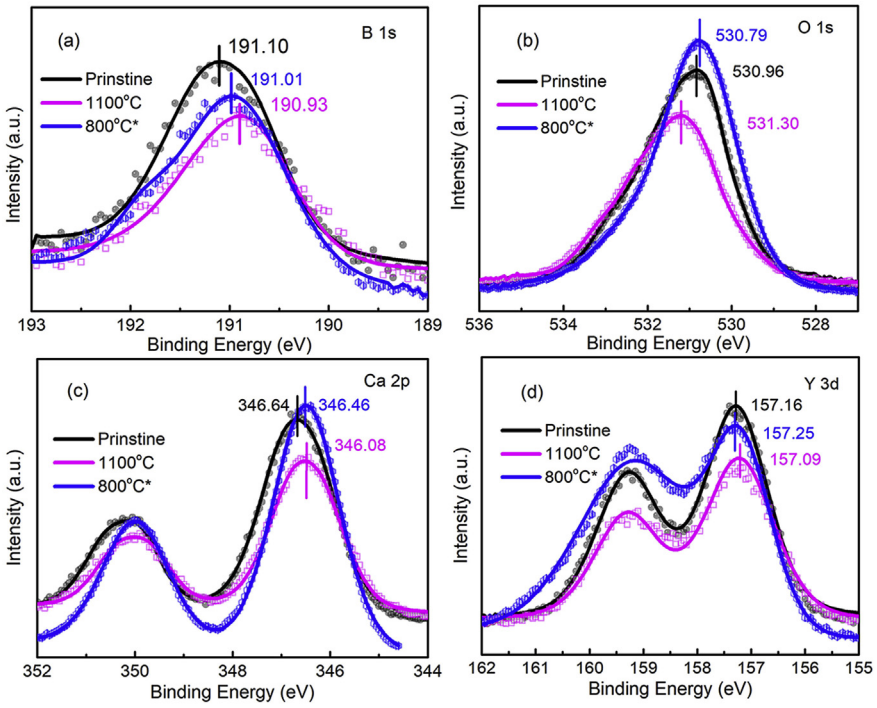

Fig. 6. Comparison of the X-ray photoelectron spectra for B 1s (a), O 1s (b), Ca 2p (c), and Y 3d (d) of the pristine, annealed (1100 °C and low partial pressure of 4×10^{-6} atm for 24 h), and thermal treated YCOB crystals (800 °C in air for 0.5 h) after annealing.

the annealed YCOB sample get compensated after thermal treatment at 800 °C in air for 0.5 h, being around 57.83%, 13.40%, 7.04% and 21.73% for the O, B, Y and Ca respectively, very close to the pristine YCOB crystal (Fig. 7). Hence, we can conclude that the oxygen atoms in YCOB crystal are easier to escape than other atoms when suffering annealing in critical conditions and can be compensated after thermal treatment in air. It is worth to mention that the increase of area percentages for B, Y and Ca is owing to the decrease of oxygen atoms. The evaporation of the atoms in YCOB crystal leads to the formation of vacancy defects, especially the oxygen vacancies [47]. From this viewpoint, the variations of electrical resistivity and dielectric permittivity of the annealed YCOB samples, as presented in Figs. 2–4, should be associated with the vacancy defects under critical conditions.

5. Theoretical studies and discussion

5.1. Vacancy formation energy analysis

The formation energies of various vacancies including V_O, V_B, V_{Ca}, and V_Y were calculated and found to be 7.41, 17.33, 21.35, and 17.07 eV respectively at the absolute temperature of 0 K. It needs to point out that there are six kinds of oxygen atoms i.e. O_1, O_2, O_3, O_4, O_5, and O_6 in YCOB crystal. The calculated vacancy formation energies for the six kinds of oxygen atoms are different, being 7.41, 6.69, 6.70, 6.86, 6.71 and 6.66 eV for O_1, O_2, O_3, O_4, O_5, and O_6, respectively. For comparison, we select the largest value of 7.41 eV as the oxygen vacancy energy in this study. It is clear that the oxygen has the lowest vacancy formation energy, indicating that the oxygen in YCOB crystal should be easier to escape than other constituent atoms. In contrast, the calcium vacancy has the highest formation energy, which is triple the formation energy of V_O, indicating that calcium is the hardest element to be lost in YCOB crystal. These results are in consistence with the area percentage variations obtained by XPS. The negative change of oxygen area percentage is assumed to be associated with the lower formation energy of V_O than the other vacancies.

5.2. Charges and the bond Mulliken population analysis

The charge variations of O 2p, B 2p, Y 4d, and Ca 4s were studied to understand the range of the electronic structure variation and the charge redistribution impacted by the oxygen vacancy in YCOB crystal. The results of the first principle calculation showed that the V_O mainly affected the electronic structure of the atoms around the oxygen vacancy V_O, as can be seen in Fig. 8. Around the oxygen vacancy, the charges of B 2p, Ca 4s, and Y 4d decreased from 0.7, 1.3 and 1.32 eV to 0.23, 1.23 and 1.05 eV, after forming an oxygen vacancy. These results indicate that the electron densities of the core atoms (B, Ca and Y) in polyhedra are increased after losing an oxygen atom, leading to the decreased binding energy values for the YCOB samples annealed at 1100 °C and low oxygen pressure (4×10^{-6} atm) for 24 h (Fig. 6 (a), (c) and (d)). Moreover, for the oxygen atoms connected with the B-O triangles, the charges of O_2 and O_3 atoms are found to increase from −0.85 ~ −0.86 to −0.83 after the formation of an oxygen vacancy at O_4 site. The decrease of electron density for oxygen atoms contributes to the increase of binding energy for O 1s, as observed in Fig. 6(b).

The bond Mulliken population analysis is a common approach to evaluate the chemical bonding strength. The larger bond population value usually corresponds to stronger chemical bonding strength [48]. It is obtained from Table 1 that the average Milliken bond population of B-O is higher than those of Y-O and Ca-O, which means that the B-O bonds are more covalent than Y-O and Ca-O. Therefore, the boron vacancies introduce relative deeper acceptor level in the band gap of YCOB. On the contrary, the chemical bonds of Ca-O and Y-O are more ionicity compared to B-O bonds, and the corresponding vacancies could introduce shallow acceptor levels, as shown in Fig. 9. Considering that the formation of oxygen vacancy mainly leads to the local structural distortion, the bond Mulliken populations and the bond angles around the oxygen vacancy were calculated to study the variations of chemical bonding strength after the formation of oxygen vacancy. Relevant results are summarized and Table 1. It is found that the Y-O, Ca-O, and B-O polyhedrons become distorted after forming an oxygen vacancy. The average bond length and the chemical bond angles in M-O (M:

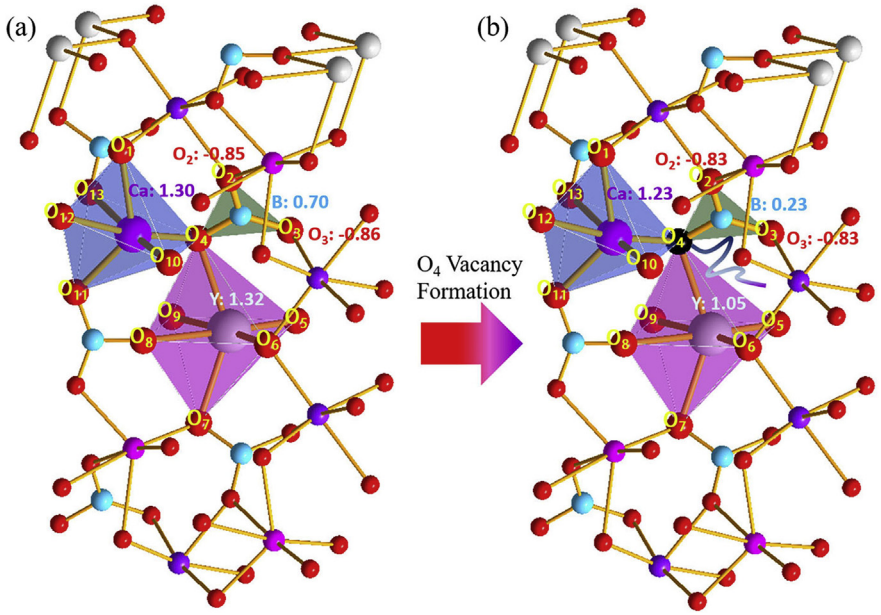

Fig. 8. Comparison of the atomic charges in YCOB crystals before (a) and after (b) losing an oxygen atom (the black ball indicates the oxygen vacancy).

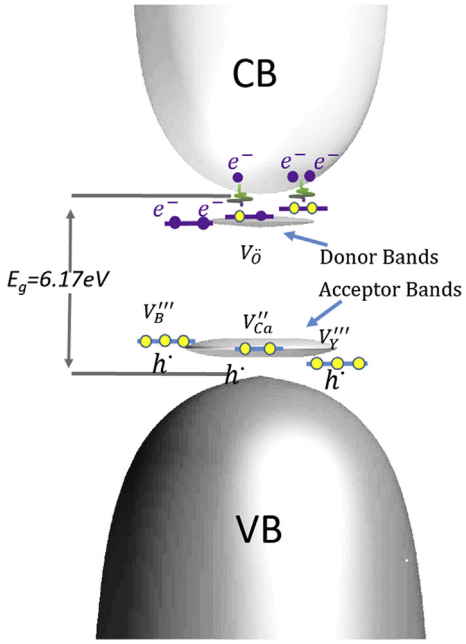

Fig. 9. Schematic energy band with vacancy defects in YCOB crystal.

Ca, Y, and B atoms) are all changed. Besides, the chemical bonding strength is decreased (obtained from the Mulliken population (|e|)), which is in agreement with the XPS results. The increased structure distortion and the decreased chemical bonding strength contributed to the polarization enhancement in the annealed YCOB crystal, accounts for the increased dielectric permittivity.

It should be noted that the first principle calculations for YCOB crystal were performed under conditions of 0 K and 0 GPa. The oxygen atoms would be easier to escape than other atoms when the crystal annealed at high-temperature of 1100 °C and low oxygen partial pressure of 4×10^{-6} atm. Therefore, the increased dielectric permittivity of YCOB crystal is contributed to the oxygen vacancy, which is expected to be amplified under the studied experimental conditions.

5.3. Effects of oxygen vacancy on electrical resistivity

The XPS results prove that all kinds of atoms would escape from the YCOB crystal and form vacancy defects (including oxygen, borate, calcium, and yttrium vacancies) under the critical conditions (high-temperature and low oxygen partial pressure). The possible vacancy defects formed in YCOB crystal are presented in Equations (6)–(9).

$$Y_Y \rightarrow V_Y''' + 3h^{\bullet} + Y \tag{6}$$

$$B_B \rightarrow V_B''' + 3h^{\bullet} + B \tag{7}$$

$$Ca_{Ca} \rightarrow V_{Ca}'' + 2h^{\bullet} + Ca \tag{8}$$

$$O_O \rightarrow V_O^{\bullet\bullet} + 2e' + \frac{1}{2}O_2\uparrow \tag{9}$$

The borate, calcium, and yttrium vacancies would bind three, two, and three hole carriers ($h^{\bullet}$) nearby, respectively, introducing acceptor levels above the valence band maximum of YCOB crystal, as shown in Fig. 9. These acceptor levels will lead to the combination of the electrons and holes, positively impact the conductivity. The change of energy band is believed to be associated with the variation of electrical properties of YCOB crystals. On one hand, the oxygen vacancy would bind two electron carriers (e') and introduce donor levels near the conduction band minimum. These electron carriers will be excited to the conduction band when absorbing activation energy. Since a large number of oxygen vacancies could be formed in the YCOB crystals under critical conditions (high-temperature and low oxygen partial pressure), the increase of electrons in the conduction band could enhance the electrical conductivity and decrease the electrical resistivity of YCOB crystal. On the other hand, the introduced donor levels in the band gap will reduce the activation energy required for exciting the electrons to the conduction band. So it is reasonable to conclude

Table 1
The variations of chemical bond lengths, Mulliken bond populations, and bond angles in YCOB crystals before and after oxygen vacancy formation.

Chemical bonds	Pristine YCOB			YCOB with oxygen vacancies		
	Bond Length(Å)	Mulliken Population (|e|)	Angles (°)	Bond Length(Å)	Mulliken Population (|e|)	Angles (°)
Ca-O_1	2.417	0.08	/	2.453	0.06	/
Ca-O_4	2.298	0.10	/	/	/	/
Ca-O_{10}	2.324	0.09	/	2.298	0.09	/
Ca-O_{11}	2.303	0.11	/	2.29	0.10	/
Ca-O_{12}	2.437	0.13	/	2.402	0.14	/
Ca-O_{13}	2.549	0.03	/	2.523	0.03	/
∠O_{10}-Ca-O_{12}	/	/	88.084	/	/	88.364
B-O_2	1.369	0.82	/	1.364	0.72	/
B-O_3	1.371	0.81	/	1.365	0.76	/
B-O_4	1.386	0.78	/	/	/	/
Y-O_4	2.326	0.26	/	/	/	/
Y-O_5	2.188	0.48	/	2.223	0.45	/
Y-O_6	2.213	0.46	/	2.239	0.43	/
Y-O_7	2.345	0.28	/	2.389	0.28	/
Y-O_8	2.296	0.27	/	2.974	0.28	/
Y-O_9	2.326	0.26	/	2.348	0.25	/
∠O_7-Y-O_5	/	/	96.769	/	/	104.369
∠O_7-Y-O_8	/	/	76.875	/	/	82.354
∠O_7-Y-O_9	/	/	76.875	/	/	97.567
∠O_5-Y-O_6	/	/	104.369	/	/	96.769

that the decreased electrical resistivity for the annealed YCOB crystal is mainly attributed to the formation of oxygen vacancies, and the recoverable electrical properties are associated with the oxygen vacancy variations at elevated temperatures in air.

6. Conclusions

The stability of electrical properties of YCOB crystal annealed under combined critical conditions (high-temperatures of 900–1100 °C and low oxygen partial pressure of 4×10^{-6} atm) was studied. The electrical resistivity of YCOB crystal shows a slight decrease after annealing, being shifted from $5 \times 10^7\ \Omega\cdot$cm (pristine sample) to $2 \times 10^7\ \Omega\cdot$cm (annealed sample) at 850 °C. In contrast, the relative dielectric permittivity shows an increase after annealing, which is associated with vacancy defects formed in the annealed YCOB crystal. Theoretical studies indicate that the oxygen atom is relative easier to escape during annealing when compared to other constituent atoms in YCOB crystal due to the lowest defect formation energy. The formation of oxygen vacancies decreases the chemical bonding strength (M-O) and provides extra donor levels near the conduction band, leading to the increased dielectric permittivity and decreased electrical resistivity for the annealed YCOB crystal. The recoverable electrical resistvity and dielectric permittivity of the YCOB crystal after thermal treatment are related to the variation of oxygen vacancy defects.

Acknowledgements

This work was financially supported by the Primary Research & Development Plan of Shandong Province (2017CXGC0413) and the National Natural Science Foundation of China (51872165).

References

[1] Zhang SJ, Yu FP. Piezoelectric materials for high temperature sensors. J Am Ceram Soc 2011;94:3153–70.
[2] Zhang SJ, Li F, Yu FP, Jiang XN, Lee HY, Luo J, et al. Recent developments in piezoelectric crystals. J Korean Cera Soc 2018;55:419–39.
[3] Turner RC, Fuierer PA, Newnham RE, Shrout TR. Materials for high temperature acoustic and vibration sensors: a review. Appl Acoust 1994;41:299–324.
[4] Zhang SJ, Fei YT, Chai BHT, Frantz E, Snyder DW, Jiang XN, Shrout TR. Characterization of piezoelectric single crystal $YCa_4O(BO_3)_3$ for high temperature applications. Appl Phys Lett 2008;92:202905.
[5] Markiewicz E, Pawlaczyk C, Pajaczkowska A, Kls A. Piezoelectric and elastic properties of γ-irradiated gadolinium calcium oxoborate, $GdCa_4O(BO_3)_3$ single crystal. Ferroelectrics 2009;389:55–62.
[6] Kumar RA, Dhanasekaran R. Nucl Instrum Methods Phys Res Sect B Beam Interact Mater Atoms 2012;287:109–12.
[7] Zheng YQ, Tu XN, Chen JJ, Gao P, Shi EW. Piezoelectric acceleration sensors based on LGX and ReCOB crystals for application above 645 ºC. 2013 Joint UFFC. In: EFTF and PFM Symp; 2013. p. 977–9.
[8] Krempl P, Schleinzer G, Wallnö Fer W. Gallium phosphate, $GaPO_4$: a new piezoelectric crystal material for high-temperature sensorics. Sensor Actuat. A-Phys 1997;61:361–3.
[9] Worsch PM, Krempl PW, Wallnofer W. $GaPO_4$ crystals for sensor applications, Sensors. Proceedings of IEEEE. Comini, Analytica Chimica Acta 2002;1:589–93.
[10] Yu FP, Hou S, Zhao X, Zhang SJ. High-temperature piezoelectric crystals $ReCa_4O(BO_3)_3$: a review. IEEE Trans Ultrason Ferroelectr Freq Control 2014;61:1344–56.
[11] Yu FP, Zhang SJ, Zhao X, Yuan DR, Wang CM, Shrout TR. Characterization of neodymium calcium oxyborate piezoelectric crystal with monoclinic phase. Cryst Growth Des; 2010. p. 1871–7.
[12] Yu FP, Zhang SJ, Zhao X, Yuan DR, Wang QM, Shrout TR. High temperature piezoelectric properties of yttrium calcium oxyborate single crystals. Phys Stat Solidi RRL 2010;4:103–5.
[13] Schulz M, Sauerwald J, Richter D, Fritze H. Electromechanical properties and defect chemistry of high-temperature piezoelectric materials. Ionics 2009;15:157–61.
[14] Damjanovic D. Materials for high temperature piezoelectric transducers. Curr Opin Solid St M 1998;3:469–73.
[15] Fritze H, Seh H, Tuller HL, Borchardt G. Operation limits of langasite high temperature nanobalances. J Eur Ceram Soc 2001;21:1473–7.
[16] Fritze H. High temperature bulk acoustic wave sensors. Meas Sci Technol 2010;22:012002.
[17] Zhang SJ, Zheng YQ, Kong HK, Xin J, Frantz E, Shrout TR. Characterization of high temperature piezoelectric crystals with an ordered langasite structure. J Appl Phys 2009;105:114107.
[18] Kim T, Kim J, Dalmau R, Schlesser R, Preble E, Jiang XN. High-Temperature electromechanical characterization of AlN single crystals. IEEE Trans Ultrason Ferroelectr Freq Control 2015;62:1880–7.
[19] Kim K, Zhang SJ, Huang WB, Yu FP, Jiang XN. $YCa_4O(BO_3)_3$ (YCOB) high temperature vibration sensor. J Appl Phys 2011;109:126103.
[20] Hou S, Yu FP, Liu YQ, Zhang SJ, Lu QM, Wang SL, et al. Crystal growth and characterization of thulium calcium oxyborate high-temperature piezoelectric crystals. CrystEngComm 2015;17:553–60.
[21] Zhang SJ, Jiang XN, Lapsley M, Moses P, Shrout TR. Piezoelectric accelerometers for ultrahigh temperature application. Appl Phys Lett 2010;96:013506.
[22] Zhang SJ, Fei YT, Frantz E, Snyder DW, Chai BHT, Shrout TR. High-temperature piezoelectric single crystal $ReCa_4O(BO_3)_3$ for sensor applications. IEEE Trans Ultrason Ferroelectr Freq Control 2008;55:2703–8.
[23] Zu HF, Wu HY, Wang QM. High-temperature piezoelectric crystals for acoustic wave sensor applications. IEEE Trans Ultrason Ferroelectr Freq Control 2016;63:486–505.
[24] Salazar G, Kim K, Zhang SJ, Jiang XN. Piezoelectric accelerometer for high temperature (1300°C) sensing. Proc SPIE 2011;8347:83471K.
[25] Johnson JA, Kim K, Zhang SJ, Wu D, Jiang XN. High-temperature acoustic emission sensing tests using a yttrium calcium oxyborate sensor. IEEE Trans Ultrason Ferroelectr Freq Control 2011;61:805–14.
[26] Jiang XN, Kim K, Zhang SJ, Johnson J, Salazar G. High-temperature piezoelectric sensing. Sensors 2014;14:144–69.
[27] Norrestam R, Nygren M, Bovin JO. Structural investigations of new calcium-Rare earth (R) oxyborates with the composition $Ca_4RO(BO_3)_3$. Chem Mater 1992;4:737–43.
[28] Ilyukhin AB, Dzhurinskii BF. Crystal structures of binary oxoborates $LnCa_4O(BO_3)_3$ (Ln: Gd, Tb, and Lu) and $Eu_2CaO(BO_3)_2$. Russ J Inorg Chem 1993;38:847–50.
[29] Yu FP, Zhang SJ, Zhao X, Guo SY, Duan XL, Yuan DR, et al. Investigation of the dielectric and piezoelectric properties of $ReCa_4O(BO_3)_3$ crystals. J Phys D Appl Phys 2011;44:135405.
[30] Kresse G, Furthmuller J. Efficiency of ab-initio total energy calculations for metals and semiconductors using a plane-wave basis set. Comput Mater Sci 1996:615–50.
[31] Kresse G, Furthmuller J. Efficient iterative schemes for ab initio total-energy calculations using a plane-wave basis set. Phys Rev B 1996;54:11169–86.
[32] Kresse G, Joubert D. From ultrasoft pseudopotentials to the projector augmented-wave method. Phys Rev B 1999;59:1758–75.
[33] Ceperley DM, Alder BJ. Ground-state of the electron-gas by a stochastic method. Phys Rev Lett 1980;45:566–9.
[34] Perdew JP, Zunger A. Self-Interaction correction to density-functional approximations for many-electron systems. Phys Rev B 1981;23:5048–79.
[35] Monkhorst HJ, Pack JD. Special point for brillouin-zone integrations. Phys Rev B 1976;13:5188–92.
[36] Mayeshiba T, Morgan D. Strain effects on oxygen vacancy formation energy in perovskites. Solid State Ionics 2017;311:105–17.
[37] Zhang SJ, Zheng YQ, Kong HK, Xin J, Frantz E, Shrout TR. Characterization of high temperature piezoelectric crystals with an ordered langasite structure. J Appl Phys 2009;105:114107.
[38] Xia HR, Wang CJ, Yu H, Chen HC, Wang M. Polarization and dipole moments of Co-doped potassium sodium strontium barium niobate crystals. J Appl Phys 1997;82:4465–8.
[39] Lu GW, Li CX, Wang WC, Wang ZH, Xia HR, Zhang HJ, et al. Lattice vibration and absorbance of Er: Yb: YCOB single crystals. Chem Phys Lett 2003;368:269–75.
[40] Wu XM, Yu JY, Ren TL, Liu LT. Micro-Raman spectroscopy measurement of stress in silicon. Microelectron J 2007;38:87–90.
[41] Monteseguro V, Hernandez PR, Vilaplana R, Manjon FJ, Venkatramu V, Errandonea D, et al. Lattice dynamics study of nanocrystalline yttrium gallium garnet at high pressure. J Phys Chem C 2014;118:13177–85.
[42] Atuchin VV, Kesler VG, Meng G, Lin ZS. The electronic structure of $RbTiOPO_4$ and the effects of the A-site cation substitution in $KTiOPO_4$-family crystals. J Phys Condens Matter 2012;24:1–6.
[43] Atuchin VV, Pokrovsky LD, Kesler VG, Maklakova NY, Voronkova VI, Yanovskii VK. Superstructure formation and X-ray photoemission properties of the $TlTiOPO_4$ surface. Surf Rev Lett 2004;11:191–8.
[44] Liu J, Duan XL, Zhang Y, Li ZQ, Yu FP, Jiang HD. Growth, electronic structure and properties of $Rb_2Ti_{1.95}Yb_{0.05}(PO_4)_3$ crystals. J Alloy Comp 2016;660:356–60.
[45] Bagusa S, Illas F, Pacchioni G, Parmigiani F. Mechanisms responsible for chemical shifts of core-level binding energies and their relationship to chemical bonding. J Electron Spectrosc 1999;100:215–36.
[46] Atuchin VV, Kesler VG, Pervukhina NV, Zhang ZM. Ti 2p and O 1s core levels and chemical bonding in titanium-bearing oxides. J Electron Spectrosc 2006;152:18–24.
[47] Tian SW, Li LL, Yu FP, Li YL, Chen FF, Duan XL, et al. Structural stability and electro-elastic property of YCOB crystal annealed in harsh environment. Appl Phys Lett 2018;113:122905.
[48] Fukushima K, Adachi H, Imoto S. Electronic state of helium atoms in nickel metal. J Nucl Mater 1986;140:106–12.

Shiwei Tian is a doctor student of Institute of Crystal Materials in Shandong University. He has been working on the single crystal growth and characterization of rare earth oxyborate piezoelectric crystal ($ReCa_4O(BO_3)_3$, ReCOB) for potential high temperature sensor application.

Fapeng Yu is an associate professor of Institute of Crystal Materials in Shandong University. He is a member of Chinese Ceramic Society, Chinese Physical Society and Acoustical Society of China. He holds 15 patents and has published more than 80 papers. His research interests are focusing on single crystal growth of piezoelectric and nonlinear optical crystals, property characterization and sensor applications.